



Improvement of Desulfurization Efficiency via Numerical Simulation Analysis of Transport Phenomena of Kanbara Reactor Process

Yong-Joon Lee^{1,2} · Kyung-Woo Yi^{1,3}

Received: 13 September 2020 / Accepted: 15 January 2021 / Published online: 4 June 2021
© The Korean Institute of Metals and Materials 2021

Abstract

The Kanbara reactor (KR) process is a mechanical stirring method that reacts hot metal with desulfurization flux; it is a widely implemented desulfurization method in contemporary steel production. This study aimed to develop a new impeller profile for improving the desulfurization efficiency of the KR process. We implemented operational data analysis, a computational fluid dynamics simulation based on the operational data and performed testing and analysis with impeller models on-site a production facility. Operational data from the production facility was gathered over a 3-year period. Seven impeller models with varying impeller blade width (top and bottom), height, inclination, and curvature (curved, straight, and combination) were simulated. The results were analyzed to determine the optimal conditions. A new impeller design was selected for on-site operational testing to investigate the in situ desulfurization efficiency over 350 charges, and the results corroborated the predictions by the numerical simulations. It is expected that the proposed process modification can be successfully used for improving industrial desulfurization efficiency.

Keywords Hot metal desulfurization · Kanbara reactor · Impeller · Steel industry · Computational fluid dynamics · Desulfurization efficiency

1 Introduction

There is a growing demand for extremely low sulfur content in steel, particularly for the production of exterior steel plates for high-end vehicles, petroleum pipelines, and liquefied natural gas ship plates [1, 2]. The desulfurization process has therefore become increasingly important to the steel industry, and desulfurization efficiency has been thoroughly studied [3–5]. Several desulfurization approaches are available for processing hot metals. One of the methods is nitrogen injection in a torpedo ladle [6]. In this method, a long injection pipeline is connected to a desulfurization flux hopper and compressed nitrogen gas is used to carry the flux to the hot metal. This method relies on gas stirring and does not

require the use of mechanical stirring. Nitrogen injection in a cylindrical ladle (vessel) may also be conducted, and this method utilizes a lance instead of a pipeline [7]. Mechanical stirring in a cylindrical ladle may also be used for desulfurization, with the desulfurization flux supplied from the flux hopper [8]. For this method, an impeller is connected to the reducing gear and a motor stirs the flux and the hot metal to facilitate the desulfurization chemical reaction.

The Kanbara reactor (KR) process is a widely used desulfurization method in the steel industry and is based on the mechanical stirring method [9–12]. The temperature drop using the KR process is lower than that in methods that use gas injection. The injected gas is usually at room temperature (approximately 20–25 °C), while the temperature of the molten metal ranges from 1300 to 1450 °C. The low-temperature gas may slightly cool the metal, resulting in reduced fluidity and desulfurization rates.

Flux dispersion behavior has been analyzed for different stages of the KR process [13, 14]. These studies involved imitation of the KR process using a small-scale (e.g., 1/8) water model with a vessel, water, impeller, motor, and particles (e.g., 12 g styrene foam particles; 2 mm average diameter; 0.03 g/cm³ density). The flux dispersion behavior during

✉ Kyung-Woo Yi
yikw@snu.ac.kr

¹ Department of Materials Science and Engineering, Seoul National University, Seoul 08826, Republic of Korea

² POSCO Gwangyang Steel Works, Gwangyang 57807, Republic of Korea

³ Research Center for Iron and Steel, RIAM, Seoul National University, Seoul 08826, Republic of Korea

impeller rotation was observed at the non-dispersion stage (initial), the transition stage (intermediate), and the complete dispersion stage (final). The relationship between the vortex depth and impeller immersion depth through the three stages was also observed. After the water model experiments, the relationships between particle dispersion and desulfurization behavior and between impeller rotation speed and sulfur concentrations were studied for 70 kg of hot metal [8].

The relationship between impeller rotation speed and desulfurization efficiency has also been investigated [14]. The study identified a specific rotational speed to achieve an effective amount of desulfurization. The effects of the flux injection gas flow rate on the desulfurization efficiency have also been studied [15, 16]. The composition of desulfurization flux has been evaluated [17, 18]. Desulfurization flux usually includes CaO, CaF₂, CaO + CaF₂, CaO + Al₂O₃ + CaF₂, CaO + Al₂O₃, CaO + SiO₂, CaC₂, and Mg.

It is not easy to directly implement suggestions from previous research to an industrial facility. Literature suggests that flux dispersion patterns during impeller rotation are dependent on the processing stage, and a meaningful increase in desulfurization efficiency is difficult to achieve without a dramatic increase in impeller rotation speed. An increase in the impeller rotation speed can be achieved by considering mechanical (e.g., reducing gear, bolt strength, carriage frame beam structure, impeller shaft strength, and ladle carriage car) and electrical aspects (e.g. motor, inverter, and power cables). However, if the rotation speed of the impeller is increased without reinforcement, the increased vibrations due to higher rotation speed can affect the mechanical integrity of the carriage frame and impeller shaft. Furthermore, higher rotation speeds will result in a higher load on the impeller motor. Most industrial facilities already use the maximum impeller rotation speed possible considering the facility's mechanical and electrical limitations.

Furthermore, while steel producers are aware that gas injection at the time of flux injection can increase the desulfurization efficiency, productivity is not the only factor to consider. There are environmental issues associated with the process, specifically the generation and release of fumes and fine dust. To overcome this, an additional blockage or wall must be built around the desulfurization facility, which incurs additional cost.

Considering these difficulties in implementing changes in field operations, this study aims to offer solutions without imposing a significant burden for the facilities. In many researches, three-dimensional (3D) modeling and computer simulation are implemented before on site testing [19–23]. In this study, optimizing the 3D profile of an impeller can affect the movement of the hot metal and the flux in the ladle by taking advantage of fluid dynamics without changing the

rotation speed of the impeller. This paper presents seven different impeller profile designs and computational fluid dynamics (CFD) simulations for sulfur concentration change and desulfurization efficiency. Process improvements suggested by the CFD simulations were applied to operating KR processes to validate the findings.

2 Experimental Data Acquisition

2.1 Structure of the In situ Desulfurization Facility

The KR processing facility was equipped with a ladle, impeller, shaft, reducer, motor, flux hopper, carriage frame (which is a supporting beam structure for stirring equipment), and hoisting system, as shown in Fig. 1. The function of each component is stated in Table 1.

2.2 Operational Condition Analysis and Data Processing

Desulfurization ($\text{CaO} + [\text{S}] \leftrightarrow \text{CaS} + [\text{O}]$) efficiency was measured for a basic impeller model (Impeller Model 1), where the operational conditions were based on a representative set of site conditions, and quantitative data for each parameter depended on daily operational conditions. The operational dataset contained values averaged over

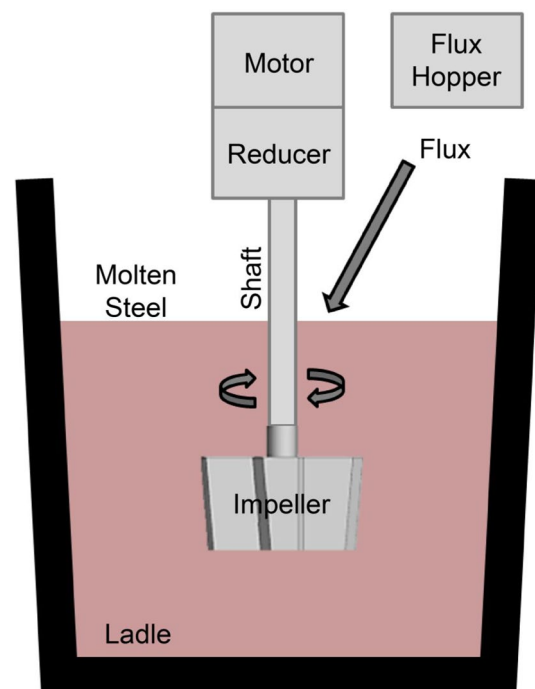


Fig. 1 Schematic diagrams of KR desulfurization

Table 1 Components of the Kanbara reactor desulfurization facility and their functions

Component	Functions
Ladle	Contains molten steel
Impeller	Stirs the molten steel with desulfurization flux
Motor	Rotates the impeller with electrical power
Carriage frame	Contains a motor and a reducer (reduces the rpm of the impeller through the motor)
Hoisting system	Moves the carriage frame vertically upwards or downwards

Table 2 Operational condition dataset for desulfurization of molten steel in the Kanbara reactor

Parameter	Data
Hot metal weight	270 ton
Hot metal density	7200 kg/m ³
Hot metal viscosity	0.07 Poise
Hot metal temperature	1350 °C
Hot metal initial sulfur concentration	0.03% (300 ppm)
Hot metal final sulfur concentration	0.003% (30 ppm)
Impeller immerge depth	650 mm
Flux chemical composition	CaO based
CaO weight (considering CaO content rate in Flux)	1548 kg
Flux injection time	250 s (started at 90 s)
Impeller rotational speed	85 rpm
Desulfurization time	600 s

36 months (abnormal operational situations were omitted), as given in Table 2.

The initial sulfur concentration of the hot metal was 0.03% (300 ppm) and was reduced to a final sulfur concentration of 0.003% (30 ppm) under the operational conditions listed in Table 2.

2.3 Three-Dimensional Modeling and Numerical Model Development

2.3.1 Three-Dimensional Modelling of KR Impeller and Ladle

The effects of seven impeller shapes were calculated to predict desulfurization efficiency during the KR process, as given in Fig. 2 and Table 3. An impeller with four blades attached to a shaft at 0°, 90°, 180°, and 270° was adopted. The top area of the impeller was larger than the bottom area, resulting in a negative incline from the top to the bottom of the impeller blades.

Impeller Model 1 was the original impeller model used in actual production lines. The parameter ‘d’ (impeller blade upper side width, mm) is described by A, ‘E’ (impeller blade bottom side width, mm) was 0.88 A, ‘b’ (impeller height,

mm) was 0.69 A, and the impeller design type was curved (for blade design). For Impeller Model 2, we increased d as 1.07 A and E as 0.97 A. Since b is limited for mold height by the factory structure, we maintained b as 0.69 A. To maintain the blade inclination degree (as 85.99°), we selected E as 0.97 A. Based on experimental data suggesting that straight impeller design type is superior to the curved type in terms of mixing time and turbulent kinetic energy [24, 25], we selected enlarged and straight type impellers for experimental Impeller Model 2.

To again verify the differences between results from the curved and straight impeller shape, we designed Impeller Model 3. For Impeller Model 3, d was 1.07 A, which is identical to that in Impeller Model 2, E was 0.97 A, b = 0.69 A, and blade inclination degree was 85.99°. The only different parameter value was the impeller design type, which was a combination of the curved and straight types. This meant that the impeller blade shape followed 50:50 interpolation points between the curved and straight type impeller blade profiles.

For Impeller Model 4, d was 1.21 A, E was 1.11 A, b was 0.69 A, and it was of straight design type. Impeller Model 4 was designed after the CFD simulation for Impeller Models 1, 2, and 3, which indicated that Impeller Model 2 achieved the highest desulfurization efficiency among them (as discussed in the results section). Thus, based on Impeller Model 2, we increased d and maintained the blade inclination degree, and as a result, E increased according to the d/E ratio. Impeller Model 5 had d as 1.35 A, E as 1.22 A, and b as 0.69 A and was also of straight design type. To consider the specifications and limits of both motor and reducer, Impeller Model 5 had maximum d and E values.

To determine the effect of blade inclination degree, we gradually reduced the inclination degree and E. Impeller Model 6 had a d of 1.07 A, which was based on Impeller Model 2, E was 0.85 A, and blade inclination degree was 80.91° (which is approximately 5° less than that of Impeller Model 2), and the design was of straight type. Impeller Model 7 had a d of 1.07, which was also based on Impeller Model 2, E was 0.76 A, blade inclination degree was 75.96° (reduced by approximately 10° than that of Impeller Model 2) and was of straight type. The top diameter of the cylindrical ladle into which molten steel was poured was 2.47 A

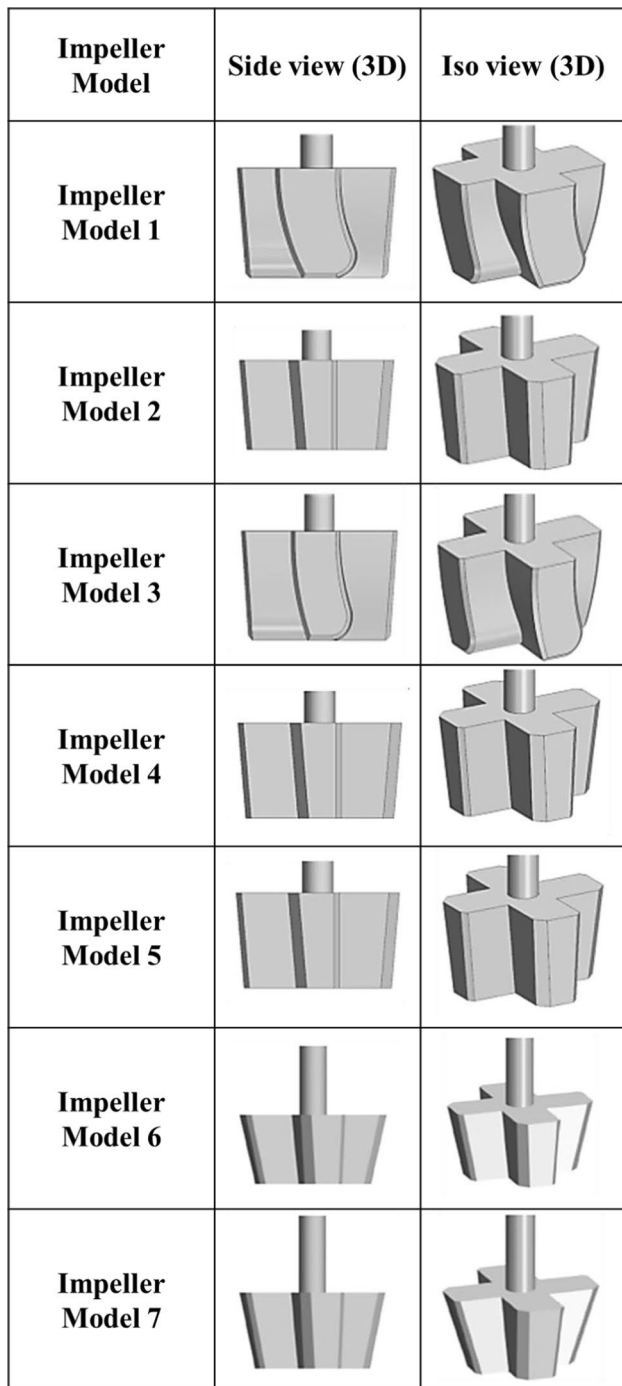


Fig. 2 Schematic diagrams of the KR desulfurization impellers

m, the bottom diameter was 2.33 A m, and the height was 3.42 A m.

2.3.2 Mesh Conditions for CFD Simulation

Mesh conditions for the 3D models are given in Table 4 and Fig. 3. Simulation was conducted using a CFD software

[Siemens Star CCM+ (version 11.04)] [26]. The parameters were as follows: mesh setting was 3D mesh, mesh type was trimmed mesh, surface mesh size was 6 to 50 mm (auto-sizing mesh), hot metal surface boundary mesh size was 25 mm (refined sized mesh), prism layer thickness was 100 mm, number of prism layers was 3, overset mesh was applied to the overlapping area of impeller and hot metal by stirring, and the number of elements was 1,700,000. A prism layer mesh is composed of orthogonal prismatic cells that usually reside next to wall boundaries in the volume mesh. They are required to accurately simulate the turbulence and heat transfer. The thickness, number of layers, and distribution of the prism layer mesh is determined by the turbulence model used. Typically, for wall function-based models, 1–3 layers are used, while for low Reynolds number and two-layer schemes, 15–25 layers are used. Moreover, overset meshes typically involve a background mesh adapted to the environment and one or more overset grids attached to bodies, overlapping with the background mesh [26].

2.3.3 Boundary Conditions for CFD Simulation

The boundary conditions for the KR desulfurization process are given in Table 5 and Fig. 4. The ladle wall and impeller body were set as wall boundaries. As the ladle top area was exposed to the ambient surroundings, a pressure boundary of 1 atm was used. The impeller overset, which is the overlapped area between the impeller stirring and hot metal stirring, was set as the overset boundary. The impeller top was set as the mass flow boundary, which controls the flux injection for the full time (0–600 s).

2.3.4 Chemical-Reaction and Physical Model Conditions for CFD Simulation

For calculating chemical reaction ($\text{CaO} + [\text{S}] \rightarrow \text{CaS} + [\text{O}]$), we used the Eddy Break-Up (EBU) reaction model in the CFD software. Multiple momentum equations for multiple phases were solved using the Eulerian multi-phase model. In the Eulerian multi-phase, phase 1 was a multicomponent liquid (pig iron comprising iron, sulfur, CaO, Ca, O^{-2} , and CaS). The numerical model conditions for the KR desulfurization process are given in Table 6. The model settings included 3D, Eulerian multi-phase, Reynolds-averaged Navier–Stokes (RANS), realizable K-Epsilon turbulence, implicit unsteady model, and Volume of Fluid (VOF) model.

The VOF model considers a single effective fluid whose properties vary according to the volume fraction of individual fluids as shown in Eq. (1).

$$\alpha_i = \frac{V_i}{V} \quad (1)$$

Table 3 Parameters and values for KR desulfurization impellers

Parameters	Impeller Model 1	Impeller Model 2	Impeller Model 3	Impeller Model 4	Impeller Model 5	Impeller Model 6	Impeller Model 7
d (Impeller blade upper side width, mm)	A	1.07 A	1.07 A	1.21 A	1.35 A	1.07 A	1.07 A
E (Impeller blade bottom side width, mm)	0.88 A	0.97 A	0.97 A	1.11 A	1.22 A	0.85 A	0.76 A
b (Impeller height, mm)	0.69 A	0.69 A	0.69 A	0.69 A	0.69 A	0.69 A	0.69 A
Blade inclination degree (°)	85.14	85.99	85.99	85.99	85.99	80.91	75.96
Impeller design type	Curved	Straight	Curved + Straight	Straight	Straight	Straight	Straight

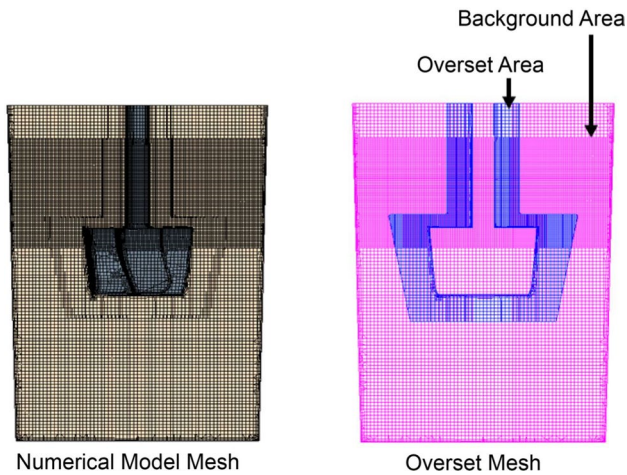
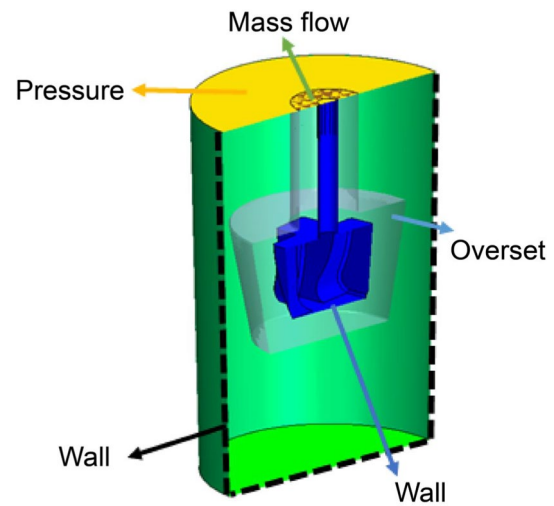
A: the value of upper side width of the present impeller blade

Table 4 Mesh conditions for the KR model

Meshing setting parameter	Data
Mesh type	Trimmed mesh
Surface mesh size	6–50 mm
Hot metal surface boundary mesh size	25 mm
Prism layer thickness	100 mm
Number of prism layers	3
Overset mesh	Overset mesh applied
Number of elements	1,700,000

Table 5 Boundary conditions for the KR model

Boundary condition setting parameter	Boundary setting value
Ladle wall	Wall boundary
Ladle top	Pressure boundary (1 atm)
Impeller body	Wall boundary
Impeller overset	Overset boundary
Impeller top	Mass flow boundary (CaO input)

**Fig. 3** Numerical model mesh and overset mesh for the KR model**Fig. 4** Boundary conditions for the KR model

where α_i is the volume fraction of phase i , V_i is the volume of phase i in the cell, and V is the volume of the cell. The volume fractions of all phases in a cell must sum up to one. The Volume of Fluid (VOF) multiphase model is a simple

multiphase model that is suited to simulating flows of several immiscible fluid mixtures, free surfaces, and phase contact time. In such cases, there is no need for extra modeling of inter-phase interaction, and the model assumption that

Table 6 Numerical model conditions for the KR model

Numerical model setting parameter	Details
Three dimensional	–
Implicit unsteady	–
Reynolds-averaged Navier–Stokes	–
Realizable K-epsilon turbulence model	–
Eulerian multi-phase	Phase 1—Multi Component Liquid Pig Iron (Iron, CaO, CaS, O, S) Eddy break-up reaction (CaO + [S] → CaS + [O]) User defined reaction rate
Volume of fluid (VOF)	Mass fraction converted

all phases share velocity, pressure, and temperature fields becomes a discretization error. Due to its numerical efficiency, the model is suited for simulations of flows where each phase constitutes a large structure, with a relatively small total contact area between phases. The spatial distribution of each phase at a given time is defined in terms of a variable that is called the volume fraction. A method of calculating such distributions is to solve a transport equation for the phase volume fraction. The distribution of phase i is driven by the phase mass conservation equation. Since we gathered data based on mass unit, we defined the two phases as the gas (air) phase and liquid (molten iron with other components) phase. Moreover, molten iron (Fe), molten CaO, molten CaS, [O], and [S] were considered as the multi-components in the liquid phase. We calculated the volume fraction using molecular volume.

For the fluid dynamics equations, the mass conservation equation for fluid i is shown as follows in Eq. (2).

$$\frac{\partial(\alpha_i \rho_i)}{\partial t} + \nabla \cdot (\alpha_i \rho_i \vec{v}) = \rho_i S_{\alpha_i} \quad (2)$$

where S_{α_i} is the source or sink term of phase i , which is due to the chemical reaction ($\text{CaO} + [\text{S}] \rightarrow \text{CaS} + [\text{O}]$), and ρ_i is the volume of phase i in the cell. The mass conservation equation for the effective fluid is obtained by summing up all component equations and using the condition shown in Eq. (3):

$$\sum_i \alpha_i = 1 \quad (3)$$

The effective fluid properties are computed according to the volume fractions, as shown in Eq. (4):

$$\rho = \sum_i \alpha_i \rho_i \quad (4)$$

Star-CCM+ calculates the volume fractions of each phase as follows. When there are two VOF phases present, the volume fraction transport is solved for the first phase only. In

each cell, the volume fraction of the second phase is adjusted so that the sum of the volume fractions of the two phases is equal to 1. When there are three or more VOF phases present, the volume fraction transport is solved for all phases. The volume fraction of each phase is then normalized based on the sum of the volume fractions of all phases in each cell [26].

The initial value setting of each of the elements were: molten iron 99.97 mass%, sulfur 0.03 mass%, CaO 0 mass%, Ca 0 mass%, O^{-2} 0 mass%, and CaS 0 mass%. The desulfurization flux (CaO) was assumed to be evenly supplied from the top of the impeller (total 1548 kg) from 90 to 340 s, as shown in Table 2.

2.3.5 Turbulent Modeling

RANS equations were used for turbulence modeling. To simulate fluid flow, the following equations were solved [27, 28].

First, the following continuity equation should be solved as Eq. (5).

$$\frac{\partial}{\partial t} \int_V \rho dV + \oint_A \rho v \cdot da = \int_V S_u dV \quad (5)$$

where t refers to the time, V is the volume, ρ is the density, A is the area, v is the velocity, and S_u is the source term. Here, the source term S_u is the mass source or sink. The dimensions of the mass source term are mass per volume per time; S_u is a mass source term related to the phase source term as shown in Eq. (6), and the dependency on the volume fractions of the constituent phases of the fluid mixture is accounted for through the density (volume weighted mixture) while solving the continuity equation.

$$S_u = \int_i S_{\alpha_i} \cdot \rho_i \quad (6)$$

Since the numerical model conditions for the KR model (Table 6) are Volume of Fluid (Volume Fraction) and the Chemical reaction calculation ($\text{CaO} + [\text{S}] \rightarrow \text{CaS} + [\text{O}]$), the mass of CaS production volume per time is the source term of the continuity equation.

The second equation is the momentum equation:

$$\int_V \rho v dV + \oint_A p v \otimes v \cdot da = - \oint_A p I \cdot da + \oint_A T \cdot da + \oint_V f_b dV + \oint_V S_u dV \quad (7)$$

where I is the identity tensor, T is the viscous stress tensor, and f_b is the resultant of the body forces (such as gravity and centrifugal forces) per unit volume acting on the continuum. Here, the source term S_u is defined as the mass source with a vector profile that specifies the momentum source, where the dimensions of the momentum source term are force per volume. Regarding the momentum source velocity derivative, momentum source is a function of velocity that sets the derivative of the momentum source with respect to the components of velocity as a vector profile value. The momentum source is mainly derived from the interfacial area between the impeller stirrer and hot metal, and the dependency of the volume fraction of the constituent phases of the fluid mixture is accounted for through the density (volume weighted mixture) while solving the momentum equation as well as the continuity equation.

The third equation is a set of energy equations.

$$\frac{\partial}{\partial t} \int_V \rho E dV + \oint_A p H v \cdot da = - \oint_A q \cdot da + \oint_A T \cdot v da + \oint_V f_b v dV + \oint_V S_u dV \quad (8)$$

where, E is the energy, H is enthalpy, and q is the heat flux per unit volume. Here, the source term S_u is the mass source with a vector profile that specifies the energy source. The energy source term dimension is the energy per volume. Regarding the velocity derivative of the energy source, it is a function of velocity that sets the derivative of the kinetic energy source with respect to the components of velocity as a vector profile value.

According to the K-Epsilon (k - ϵ) model, turbulent kinetic energy (TKE, in kJ/kg) is the mean kinetic energy per unit mass associated with eddies in turbulent flow [29–34] and is defined in Eq. (9) [35, 36]:

$$k \equiv \frac{1}{2} \langle u_i \cdot u_i \rangle = \frac{1}{2} [u_1^2 + u_2^2 + u_3^2] \quad (9)$$

where u_1 , u_2 , and u_3 are the velocity components (m/s) in a generalized coordinate system.

In this study, we discuss the TKE for post-processing in the CFD simulation. A relevant equation for the TKE is [35]:

$$\rho \frac{\partial k}{\partial t} = \frac{\partial}{\partial x_j} \left[\left(\mu + \frac{\mu_t}{Pr_k} \right) \frac{\partial k}{\partial x_j} \right] + \left(2\mu_t S_{ij} - \frac{2}{3} \rho k \delta_{ij} \right) - \frac{C_D \rho k^{\frac{3}{2}}}{l} \quad (10)$$

where the left-hand side is the rate of increase in kinetic energy (k), and the right-hand side is the diffusion rate of k ,

the generation rate of k , and the dissipation rate for k .

Another relevant equation is the dissipation rate equation [35]:

$$\rho \frac{\partial \epsilon}{\partial t} = \frac{\partial}{\partial x_j} \left[\left(\mu + \frac{\mu_t}{Pr_k} \right) \frac{\partial \epsilon}{\partial x_j} \right] + C_{\epsilon 1} \frac{\epsilon}{k} \left(2\mu_t S_{ij} - \frac{2}{3} \rho k \delta_{ij} \right) \frac{\partial u_i}{\partial x_j} - C_{\epsilon 2} \rho \frac{\epsilon^{\frac{3}{2}}}{k} \quad (11)$$

where C_D is the dissipation coefficient, l is the mixing length, μ is the coefficient of viscosity, μ_t is the eddy viscosity, Pr is the Prandtl number, S_{ij} is $(2\Omega_{ij}\Omega_{ij})^{1/2}$, and Ω_{ij} is $\frac{1}{2} \left(\frac{\partial u_i}{\partial x_j} - \frac{\partial u_j}{\partial x_i} \right)$, ϵ is dissipation the rate, t is the time, and $C_{\epsilon 1}$, $C_{\epsilon 2}$ are k - ϵ model constants.

2.3.6 Miscellaneous Topics for Numerical Simulations

The implicit unsteady model of Star-CCM+ uses variable time-steps to accommodate unevenly spaced time levels. The basic formula is:

$$\frac{d}{dt} (\rho \varphi V) = \frac{(\rho \varphi V)^{n+1} - (\rho \varphi V)^n}{\Delta t} \quad (12)$$

where φ is the value of the selected scalar, Δt is time difference, n is the previous time level, and $n+1$ is the current time level.

We modified the reaction rate coefficient in CFD such that the initial sulfur concentration in molten steel [S] of 300 ppm decreased to 30 ppm in an operation time of 600 s for the reference impeller design (Impeller Model 1). We used the EBU reaction models [26] for physical model setting. The EBU model is intended for modeling reacting flow with fast chemistry reactions where the reaction rate is determined by the rate at which turbulence can mix the reactants and heat. EBU models characterize the reacting flow system with a specified number of species, chemical reactions, and kinetic reaction rate by the turbulent mixing rate [26]. We modified the EBU reaction rate coefficient (A) using Eq. (13) to match the final concentration of 30 ppm after desulfurization for 600 s using Impeller

Model 1. After achieving the modified ‘A’ value (1.128), we used it for CFD simulations of Impeller Models 2 to 7.

$$\text{Eddy-Break-Up reaction rate coefficient} = A \times (\text{desulfurization reaction rate, } f(\text{time})) \quad (13)$$

The sulfur concentration analysis is set to be calculated for the time period of 0–600 s. Sulfur concentration in molten steel [S] (mass%) is shown in Eq. (14).

$$\begin{aligned} [\text{S}](\text{mass}\%) &= \frac{\text{total mass of sulfur}}{\text{total mass of molten steel}} \\ &= \frac{\text{density of sulfur} \times \text{total volume of sulfur}}{\text{density of molten steel} \times \text{total volume of molten steel}} \times 100 \end{aligned} \quad (14)$$

The time interval for CFD was set as 0.01 s with 10 iterations for each 0.01 s.

2.3.7 Validation of CFD Simulation Model

We verified the CFD simulation model for the KR desulfurization process. Based on the actual processing data acquired over 36 months using Impeller Model 1, we set some of the parameter values as follows. The desulfurization time was set to 600 s, the impeller stirring starts at 90 s, the initial sulfur concentration was 300 ppm, and the final sulfur concentration was 30 ppm. Using Impeller Model 1, we plotted a reverse-exponential type curve that showed a sulfur concentration value of 300 ppm from 0 to 90 s and 30 ppm by 600 s. We incorporated the parameters of the theoretically validated curve into the CFD software and projected the data into the chemical reaction coefficient table ($\text{CaO} + [\text{S}] \rightarrow \text{CaS} + [\text{O}]$). Since CaS covered CaO after the desulfurization chemical reaction, CaO was positioned inside of CaS, implying that it could not collide and react with [S]; the reaction rate reduced as time progressed. We used a trial and error method to match the final sulfur concentration to the actual averaged data (sulfur concentration was 30 ppm at 600 s). Based on the CFD simulation results of the Impeller Model 1, we modified the values of the other parameters and the 3D modeling profile of impeller and achieved explainable results for Impeller Model 2–7; the range of the final sulfur concentration was 19–49 ppm.

3 Results and Discussion

3.1 Numerical Analysis for Sulfur Concentration Comparison from Impeller Models

The sulfur concentration analysis was conducted for seven impeller models, as shown in Fig. 2 and Table 3. The

initial sulfur concentration (at $t = 0$ s) in the hot metal for all impeller models was the same (300 ppm; weight

percentage of 0.03%). However, the final sulfur concentration values (at $t = 600$ s) in the hot metal differed for all impeller models (Impeller Model 1: 0.0030 (30 ppm),

Impeller Model 2: 0.0026 (26 ppm), Impeller Model 3: 0.0028 (28 ppm), Impeller Model 4: 0.0019 (19 ppm), Impeller Model 5: 0.0023 (23 ppm), Impeller Model 6: 0.0036 (36 ppm), and Impeller Model 7: 0.0049 (49 ppm), as shown in Fig. 5.

For a comparison between Impeller Models 1 and 2, the parameters that differed were impeller blade width and impeller design type (curved or straight profile). The final [S] for Impeller Model 1 was 30 ppm (by mass) and the final [S] for Impeller Model 2 was 26 ppm (by mass). This indicated that the final sulfur concentration decreased as the width of the impeller blade increased. However, we thought that this comparison did not include the impeller design type. We therefore could not find out whether the curved or straight impeller blade profile is more efficient for desulfurization. To compensate for this, we compared Impeller Models 2 and 3. The only difference between these models was the impeller design type. The final [S] values for Impeller Models 2 and 3 were 26 and 28 ppm (by mass), respectively. Hence, we concluded that an impeller of the straight type is more efficient for desulfurization than the curved type.

Based on Impeller Model 2 (d: 1.07a mm), we increased the width of the impeller blades for Impeller Models 4 (d: 1.21a mm) and 5 (d: 1.35a mm). The final [S] for Impeller

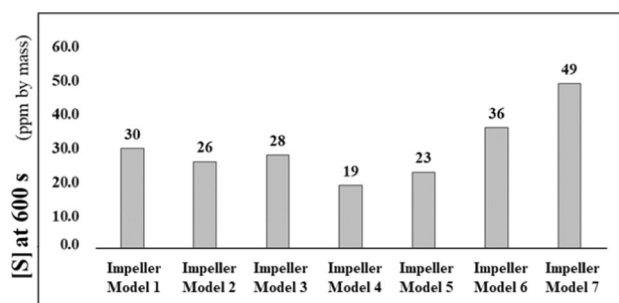


Fig. 5 Sulfur concentration analysis at 600 s for the KR model

Model 4 was 19 ppm (by mass). The results obtained were consistent with the earlier results, i.e., the final sulfur concentration reduced as the blade width increased.

However, Impeller Models 4 and 5 did not display this tendency. In contrast, the final sulfur concentration of Impeller Model 5 was 23 ppm (by mass). Since the top diameter of the hot metal ladle was 2.47a mm and the bottom diameter was 2.33a mm, we can conclude that the average diameter of the ladle was 2.40a mm. The ratios of the upper side widths of the impeller blades to the average diameter of the ladle were 0.50 and 0.56 for Impeller Models 4 and 5, respectively. Hence, we concluded that the lowest sulfur final concentration could be achieved when the ratio of the upper side widths of the impeller blade to the average diameter of the ladle was approximately 0.5. Comparisons between Impeller Models 4 and 5 are discussed in detail in the next section.

Based on Impeller Model 2 (blade inclination degree: 85.99°), we reduced the blade inclination degree for Impeller Models 6 (blade inclination degree: 80.91°) and 7 (blade inclination degree: 75.96°). On reducing the inclination degree, the blade contact surface for the movement of hot metal was decreased.

The blade contact surface areas of Impeller Models 2, 6, and 7. The blade area calculation results were 0.35, 0.33, 0.31 A² for Impeller Models 2, 6, and 7, respectively. Compared with Impeller Model 2, the area for Impeller Models 6 was 94.1% and 88.0%, respectively. The CFD results indicated that the final sulfur concentration was 26, 36, and 49 ppm (by mass) for Impeller Models 2, 6, and 7, respectively. The desulfurization efficiency for Impeller Models 2, 6, and 7 was 8.4%, 8.1% and 7.7% (which is 91.7% of Impeller Model 2), respectively. The area difference was approximately 6% for each model while the desulfurization efficiency difference was about 0.35%. There was, therefore, a linear relationship between area difference and desulfurization efficiency. From these results, a decrease in the inclination degree turned out to be relatively less efficient for desulfurization.

3.2 Effects of Velocity Magnitude, Turbulent Kinetic Energies, and Streamline on Final Sulfur Concentration

The velocity magnitude (m/s) was calculated for the time period ranging from 0 to 600 s (the final moment of desulfurization). In this study, the velocity magnitude is defined as the square root value of the summation of the squares of the velocities in the x-, y-, and z-directions, as shown in Eq. (15).

$$v = \sqrt{v_x^2 + v_y^2 + v_z^2} \quad (15)$$

The average velocities for the impellers were as follows: 1.581, 1.869, 1.845, 2.616, 3.429, 1.223, and 0.990 m/s for Impeller Models 1, 2, 3, 4, 5, 6, and 7 at 600 s, respectively, as shown in Table 7 and Fig. 6.

The velocity analysis indicates that the final sulfur concentration at 600 s tends to decrease as the velocity is increased.

The turbulent energy value was calculated for the seven impeller models. The TKE was graphed at 600 s for comparison across the seven different impeller types (Fig. 2; Table 3). The average TKE magnitudes of the different impellers were 0.149, 0.186, 0.213, 0.261, 0.365, 0.109,

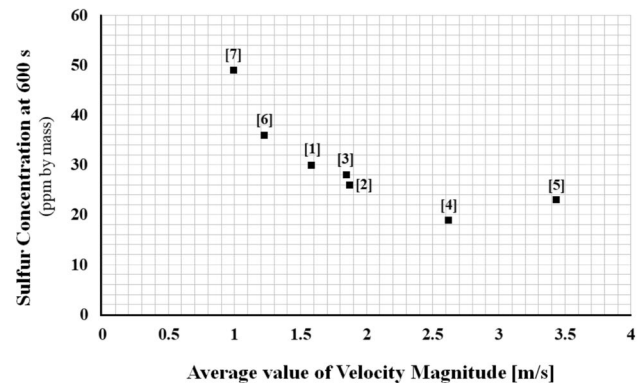


Fig. 6 Sulfur concentration analysis at 600 s with velocity values for the KR model

Table 7 Comparison among velocity magnitude, turbulent kinetic energy, sulfur concentration at 600 s, and desulfurization efficiency for impeller models

Impeller Model	Velocity magnitude (Avg., m/s)	Turbulent kinetic energy (Avg., J/kg)	Sulfur concentration at 600 s (ppm by mass)	Desulfurization efficiency (%)
1	1.581	0.149	30	8.3
2	1.869	0.186	26	8.4
3	1.845	0.213	28	8.3
4	2.616	0.261	19	8.6
5	3.429	0.365	23	8.5
6	1.223	0.109	36	8.1
7	0.990	0.093	49	7.7

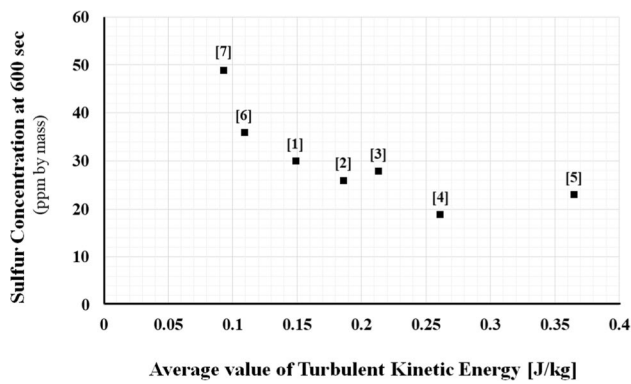
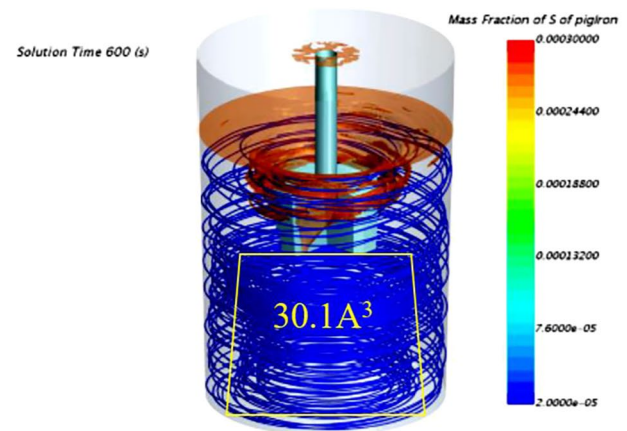


Fig. 7 Sulfur concentration analysis at 600 s with TKE values for the KR model

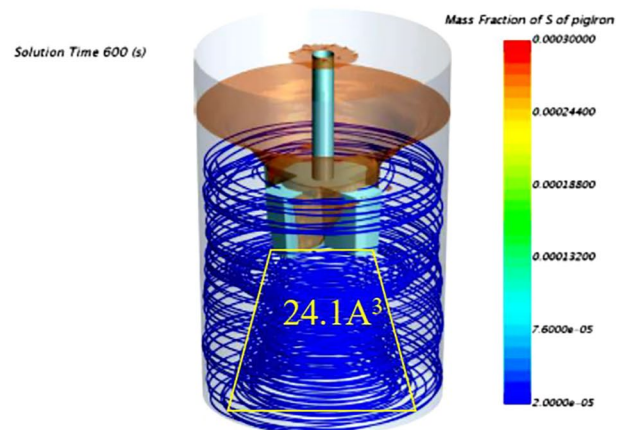
and 0.093 J/kg for Impeller Models 1, 2, 3, 4, 5, 6, and 7 at 600 s, as shown in Table 7 and Fig. 7. The TKE analysis indicates that the final sulfur concentration at 600 s tends to decrease as the TKE is increased. Hence, from the data, we discovered that turbulent kinetic energy tends to increase as velocity magnitude increases, while final sulfur concentration tends to decrease as the TKE and velocity magnitude increase.

Comparing Impeller Models 4 and 5, even though the TKE of Impeller Model 5 was higher than that of Impeller Model 4, its final sulfur concentration was also higher. For the comparison between Impeller Models 4 and 5, we analyzed a streamline of the desulfurization flux. This streamline allows for tracking of desulfurization movement, and as the streamline is distributed to different areas, the chemical reaction possibility increases. From the streamline analysis, we calculated the developing chemical reaction volume using the streamline area. For Impeller Model 4, the upper diameter was 1.7 A, the bottom diameter 1.8 A, and height 1.565 A, while for Impeller Model 5, the upper diameter was 1.33 A, the bottom diameter 1.8 A, and height 1.565 A. Thus, the resulting area for desulfurization flux distribution was 2.74 A² for Impeller Model 4 and 2.45 A² for Impeller Model 5. The volume for the resultant streamline area was 30.1 A³ for Impeller Model 4 and 24.1 A³ for Impeller Model 5 (which is 79.9% value compared with Impeller Model 4) as shown in Fig. 8.

There was also a difference in the impeller radial direction mixing area. Since the inner diameter of the ladle was 2.4 A, the impeller diameters of Impeller Models 4 and 5 were 1.21 and 1.35 A, the area for the ladle (vessel) was 4.52 A², and the rotating areas for Impeller Models 4 and 5 were 1.15 and 1.43 A², respectively. Thus, the area of impeller radial direction mixing for Impeller Model 4 was 3.37 A² and that of Impeller Model 5 was 3.09 A². Since impeller height was the same at 0.69 A, the volume of the impeller



(a) Impeller Model 4



(b) Impeller Model 5

Fig. 8 Desulfurization flux streamline analysis at 600 s for the KR model

radial direction mixing was 2.33 A³ for Impeller Model 4 and 2.13 A³ for Impeller Model 5 (which is 91.7% of that of Impeller Model 4).

3.3 Applications to Field Operations

To compare the field operational results, we could not simply compare the final sulfur concentrations, because the initial concentrations and amounts of flux differ from each other in field operations. The difference is derived from the CFD parameters that we set as representative values, which were averages taken from actual operation. From the results obtained from the final sulfur concentration of the CFD simulation, we calculated the desulfurization efficiency (%) values, as presented in Table 7. The desulfurization efficiency is defined using Eq. (16):

Desulfurization efficiency(%)

$$= \frac{\text{Atomic weight}_{\text{CaO}} \times \text{Weight}_{\text{Pigiron}} \times ([S]_{\text{initial(mass\%)}} - [S]_{\text{final(mass\%)}})}{\text{Atomic weight}_S \times \text{CaO Content rate in Flux} \times \text{Weight}_{\text{Flux}}} \times 100 \quad (16)$$

The numerical simulation study showed that three conditions can obtain better desulfurization efficiency than the original design, namely Impeller Models 2, 4, and 5. Among them, Impeller Model 4 can obtain the highest desulfurization efficiency. Impeller Model 4 was selected for field facility testing over 350 charges. The average desulfurization efficiency of Impeller Model 1 (the original model of actual production lines) for in situ charges was 7.8%. Impeller Model 4 achieved a desulfurization efficiency of 8.9%, and this value is calculated as a 14% higher desulfurization efficiency. Thus, this new design (Impeller Model 4) has been adopted for the KR process in POSCO's Gwangyang works.

4 Conclusion

Literature on desulfurization efficiency using various types of 3D impeller models suggests that systems with a higher desulfurization efficiency require a lower amount of desulfurization flux. The study began by developing a digital simulation of a KR facility using CFD software and was based on an in situ facility's operational data over 36 months. Analysis of the digital models included 3D modeling, boundary condition setting, meshing, and time-transition based CFD simulation (unsteady analysis).

Seven KR impeller models were developed for desulfurization using the simulation model. The impeller design parameters included impeller blade upper side width (d), impeller blade bottom side width (E), blade inclination degree, and impeller design type. Calculation results were obtained for sulfur concentration, desulfurization ratio, desulfurization efficiency, velocity, streamline, and TKE. Lastly, Impeller Models 1 and 4 were tested in an in situ facility to verify the CFD simulation results.

An enhancement of desulfurization efficiency means a reduction of flux during the desulfurization process. The desulfurization efficiencies of seven impeller profiles were analyzed using operational data from hot metal desulfurization conducted in an operating facility. From the numerical analysis of the sulfur concentration comparison from the impeller models, we concluded that desulfurization efficiency increases as the width of the impeller blade increases, inclination degree increases, and the blade contact surface increases. Moreover, we found that the straight blade type is more efficient than the curved blade type.

The TKE analysis and velocity magnitude analysis indicated that TKE exhibited an increasing trend as velocity

magnitude increased and that desulfurization efficiency also increased as both TKE and velocity increased. The desulfurization efficiency differed among the seven impellers as follows: Impeller Model 1: 8.3%; Impeller Model 2: 8.4%; Impeller Model 3: 8.3%; Impeller Model 4: 8.6%; Impeller Model 5: 8.5%; Impeller Model 6: 8.1%; Impeller Model 7: 7.7%.

Comparing Impeller Models 4 and 5, even though the TKE of Impeller Model 5 was higher than that of Impeller Model 4, its final sulfur concentration was also higher. For the comparison between Impeller Models 4 and 5, we analyzed a streamline of the desulfurization flux. As the streamline is distributed to different areas, the chemical reaction possibility increases. We calculated the developing chemical reaction volume using the streamline area. The volume for the resultant streamline area was 30.1 A³ for Impeller Model 4 and 24.1 A³ for Impeller Model 5 (which is 79.9% value compared with Impeller Model 4) as shown in Fig. 8. And the area of impeller radial direction mixing for Impeller Model 4 was 3.37 A² and that of Impeller Model 5 was 3.09 A². Since impeller height was the same at 0.69 A, the volume of the impeller radial direction mixing was 2.33 A³ for Impeller Model 4 and 2.13 A³ for Impeller Model 5 (which is 91.7% of that of Impeller Model 4). From these results, we found that the desulfurization efficiency increases as the chemical reaction volume increases.

The experimental and numerical results were well-correlated, as seen when Impellers Model 1 and 4 (which is the most efficient impeller model from the CFD simulation) were tested in an in situ facility. The simulated average desulfurization efficiency for Impeller Model 1 was 8.3%, and the in situ efficiency achieved across 350 charges was 7.8%. The simulated average desulfurization efficiency for Impeller Model 4 was 8.6%, and the in situ efficiency achieved was 8.9%. These figures were similar to the CFD simulation predictions for desulfurization efficiency based on the given in situ facility data. The small difference between the 3D CFD simulation and the in situ facility testing was due to variations in the impeller rpm, which was set at 85 for the CFD simulation, but varied from 80 to 145 rpm during the 350 charges in situ.

To improve the desulfurization efficiency of the KR process, we performed a numerical simulation using different impeller shapes. Based on the numerical simulation, we found that the desulfurization efficiency tended to increase as both the TKE and velocity increased. From the numerical simulation analysis, several shapes of impeller were found

to achieve better desulfurization results. Among the numerical results, the best condition was implemented to the field operations and the new condition increased the desulfurization efficiency by 14%. The improved impeller models were tested during industrial KR processing over a long time period, and this study provides compelling evidence for the long-term applicability of the process parameters presented. In this multi-parametric study, we investigated a widely optimized impeller design to provide an enhanced desulfurization efficiency and desulfurization ratio, and it is expected that the designs will have a notable effect if used in the steel industry. The results of this study firmly suggest that these novel KR desulfurization impellers would perform well.

References

- H.L. Kim, S.H. Park. *Met. Mater. Int.* **26**, 14 (2020)
- N. Saeidi, M. Jafari, J.G. Kim, F. Ashrafizadeh, H.S. Kim, *Met. Mater. Int.* **26**, 168 (2020)
- L.E.K. Holappa, *Int. Met. Rev.* **27**, 53 (1982)
- E.T. Turkdogan, *Ironmak. Steelmak.* **15**, 311 (1988)
- A. Ghosh, *Secondary Steelmaking* (CRC Press, Boca Raton, 2001), pp. 187–224
- N. Kikuchi, S. Nabeshima, Y. Kishimoto, *ISIJ Int.* **52**, 10 (2012)
- F. Oeters, W. Pluschkell, E. Steinmetz, H. Wilhelmi, *Steel Res.* **59**, 19 (1988)
- Y. Nakai, I. Sumi, H. Matsuno, N. Kikuchi, Y. Kishimoto, *ISIJ Int.* **50**, 403 (2010)
- M. Iwasaki, M. Matsuo, *Change and Development of Steelmaking Technology*, (Nippon Steel Technical Report No. 101, 2012)
- J.E. Ostberg, *Giesserei* **53**, 816 (1966)
- F. Kraemer, J. Mots, K. Rohrig, *Giesserei* **55**, 145 (1968)
- K. Kanbara, T. Nisugi, O. Shiraishi, T. Hatakeyama, *Tetsu-to-Hagané* **58**, 34 (1972)
- K. Takahashi, K. Utagawa, H. Shibata, S. Kitamura, N. Kikuchi, Y. Kishimoto, *ISIJ Int.* **52**, 10 (2012)
- Y. Nakai, I. Sumi, N. Kikuchi, Y. Kishimoto, Y. Miki, *ISIJ Int.* **53**, 1411 (2013)
- Y. Nakai, Y. Hino, I. Sumi, N. Kikuchi, Y. Uchida, Y. Miki, *ISIJ Int.* **55**, 1398 (2015)
- Y. Nakai, Y. Hino, I. Sumi, N. Kikuchi, Y. Uchida, K. Tanaka, Y. Miki, *Tetsu-to-Hagané* **102**, 443 (2016)
- Y. Nakai, N. Kikuchi, Y. Miki, Y. Kishimoto, T. Isawa, T. Kawashima, *ISIJ Int.* **53**, 1020 (2013)
- V.D. Eisenhüttenleute, *Slag Atlas* (Verlag Stahleisen mBH, Düsseldorf, 1981)
- T. Brlić, S. Rešković, I. Jandrić, *Met. Mater. Int.* **26**, 179 (2020)
- S.M. Alavizadeh, K. Abrinia, A. Parvizi, *Metals Mater. Int.* **26**, 260 (2020)
- J.-S. Nam, E. Park, J.-H. Sel, *Met. Mater. Int.* **26**, 491 (2020)
- A. Sim, E.-J. Chu, D.-W. Cho, *Met. Mater. Int.* **26**, 1207 (2020)
- J.R. Xavier, *Metals Mater. Int.* **26**, 1679 (2020)
- R.A. Ghotli, M.S. Shafeeyan, M.R. Abbasi, A.A.A. Raman, S. Ibrahim, *Chem. Eng. Process.* **148**, 107794 (2020)
- T. Yamamoto, A. Suzuki, S.V. Komarov, Y. Ishiwata, *J. Mater. Process. Tech.* **261**, 164 (2018)
- Siemens, *Star-CCM+ v11.04 (CFD Software) user-guide*, 109–7806 (2018)
- CFD-ACE+ version 2011.0 Modulus Manual, 14–172 (2011)
- F.M. White, *Fluid Mechanics*, 6th edn. (McGraw Hill, New York, 2007), pp. 130–228
- T. Debroy, A.K. Mazumdar, D.B. Spalding, *Appl. Math. Model.* **2**, 146 (1978)
- J. Szekely, N.H. El-Kaddah, J.J. Grevet, in *Proceedings of 2nd International Conference on Injection Metallurgy*, Lulea, Sweden, Paper No. 5 (1980)
- D. Mazumdar, R.I.L. Guthrie, *Appl. Math. Model.* **10**, 25 (1985)
- D.B. Spalding, in *Recent Advances in Numerical Methods in Fluids*, ed. C. Taylor, K. Morgan (Pineridge Press, Swansea, 1980), pp. 139–167
- Y. Sahai, R.I.L. Guthrie, *Metall. Trans.* **13B**, 125 (1982)
- D. Mazumdar, *Metall. Trans.* **20B**, 967 (1989)
- J.C. Tannehill, D.A. Anderson, R.H. Pletcher, *Computational Fluid Mechanics and Heat Transfer*, 2nd edn. (Taylor and Francis Inc, Routledge, 1997)
- I.B. Celik, *Introductory Turbulence Modeling* (Mechanical and Aerospace Engineering Dept, West Virginia University, Morgantown, 1999)

Publisher's Note Springer Nature remains neutral with regard to jurisdictional claims in published maps and institutional affiliations.